JOURNAL OF GEOPHYSICAL RESEARCH, VOL. 105, NO. A3, PAGES 5507–5516, MARCH 1, 2000

Quasi-linear ion cyclotron heating in the near-Earth magnetotail

C. C. Chaston

Space Sciences Laboratory, University of California, Berkeley

Y. D. Hu and B. J. Fraser

Physics Department, University of Newcastle, New Castle, New South Wales, Australia

Abstract. Quasi-linear studies in the near-Earth (X_{GSE}>-25 R_E) central plasma sheet and plasma sheet boundary layer indicate that the ion cyclotron proton anisotropy instability may lead to significant ion heating in these regions. Saturation of the anisotropy instability can yield both narrow and broadband magnetic spectra below the proton gyrofrequency with amplitudes of the order of 1 nT. These waves then heat thermal and suprathermal He^+ and O^+ ions via resonant and nonresonant processes to energies above 1 keV for He^+ ions and up to 100 eV for O^+ ions. He^{++} ions also experience significant heating to temperatures that may exceed that of the unstable proton component. These results are consistent with in situ observations of magnetic noise and heavy ion distributions in the near-Earth magnetotail.

1. Introduction

The properties of the plasma constituting the near-Earth magnetotail were first studied by *Bame et al.* [1967]. Since then observations most notably from ISEE, AMPTE, and Geotail have identified four distinct plasma domains including the magnetotail boundary layer (which includes the low-latitude boundary layer), the magnetotail lobes, the plasma sheet boundary layer, and the central plasma sheet. Of these the later two are relevant in the study of ion cyclotron heating since distributions here may be sufficiently anisotropic in this high β plasma to excite the ion cyclotron anisotropy instability and observations of electromagnetic waves below the proton cyclotron frequency in these regions are common [*Bauer et al.*, 1995].

Particle distributions in the plasma sheet boundary layer are dominated by field-aligned counterstreaming proton beams with flow speeds of the order of 1000 km/s and temperatures of the order of 1-5 keV [*Eastman et al.*, 1984]. It is well known that these distributions can excite a number of electrostatic and electromagnetic instabilities [*Grabbe and Eastman*, 1984; *Akimoto and Omidi*, 1986; *Angelopoulos et al.*, 1989; *Gary and Winske*, 1990; *Winske and Omidi*, 1992; *Chaston et al.*, 1994] including the Doppler-shifted ion cyclotron anisotropy or ion-beam anisotropy instability. This instability leads to magnetic noise bursts (MNBs) with frequencies below the local proton gyrofrequency (Ω_p).

Particle distributions in the central plasma sheet are typically described as hot and close to isotropic with temperatures and densities increasing toward the neutral sheet [*Huang and Frank*, 1994]. However, these distributions often exhibit deviations from isotropy [*Frank et al.*, 1996] due to adiabatic particle motion with changes in magnetic field topology and nonadiabatic particle motion [*Speiser and Martin*, 1995; *Ashour-Abdalla*, 1996]. These variations have been shown to excite the ion cyclotron anisotropy instability [*Chaston et al.*, 1999a] also leading to MNBs with frequency < Ω_p.

Copyright 2000 by the American Geophysical Union.

Paper number 1999JA900466.
0148-0227/00/1999JA900466$09.00

Studies of ion composition using ISEE 1 data collected in the near-Earth central plasma sheet and plasma sheet boundary layer indicate significant densities of antisunward flowing heavy ions of ionospheric origin. In the plasma sheet boundary layer, *Eastman et al.* [1984] reports He^+/H^+ density ratios of < 0.05 and O^+/H^+ ratios of 0.1 to 0.43 during active times with proton densities from 0.073 to 0.425 cm^{-3}. *Lennartson and Shelley* [1986] find that central plasma sheet ions are mainly of solar wind origin (H^+ and He^{++}) with average ion densities and energies per nucleon across the central plasma sheet of 0.5-1 cm^{-3} and 2-4 keV consistent with the earlier results of *Petersen et al.* [1981] and *Sharp et al.* [1982]. The corresponding ion density and energy of the O^+ and H^+ ionospheric components are 0.01-0.05 cm^{-3} and 3-5 keV and 0.0001-0.005 cm^{-3} and 3-4 keV, respectively, also consistent with the findings of *Eastman et al.* [1984]. Significantly, the He^+ and O^+ ions are observed with broad energy and pitch angle distributions inconsistent with acceleration of a cold ionospheric population through a potential drop alone [*Lennartsson et al.*, 1985]. This is particularly true when adiabatic particle motion is considered in the decreasing magnetic field from the high-latitude ionosphere to the plasma sheet.

In addition to the warm ionospheric and solar wind components discussed above, a significant density of cold-warm antisunward streaming ionospheric ions composed of either O^+ or H^+ exists throughout the central plasma sheet. A typical density for these components is 0.004 cm^{-3} with energies of the order of 100 eV [*Sharp et al.*, 1981, 1983; *Eastman et al.*, 1984; *Delcourt et al.*, 1993, 1994]. More recently, observations from the Geotail spacecraft have identified warm He^+ and O^+ beams in the central plasma sheet and its boundary layer [*Frank et al.*, 1996] and cold He^+ and O^+ beams in the magnetotail lobe/mantle [*Hirahara et al.*, 1996; *Seki et al.*, 1999].

Ion heating in the auroral acceleration region with or without further acceleration through a parallel potential drop [*Mozer et al.*, 1980] and upflowing ions in the polar wind with acceleration through a parallel potential drop have long been considered as possible source mechanisms for energetic distributions of ionospheric ions observed in the magnetotail. A review of heating processes and observations in the aurora is given by *Andre and Yau* [1997]. While this explanation is adequate for the cold closely field-

aligned beams discussed above, it is not alone sufficient to account for the broad pitch angle and energy spectra often observed. In this report, we demonstrate self-consistently how ions of ionospheric and solar wind origin found in the central plasma sheet and its boundary layer may be locally heated to the observed thermal energies by the broadband electromagnetic turbulence ubiquitous throughout these regions.

2. Quasi-linear Equations

The formalism implemented is the fluid-kinetic approach of *Chaston et al.* [1999b] where it is assumed that each component maintains a bi-Maxwellian functional form throughout the heating process and the instability saturates linearly. This technique is similar to that adopted by *Davidson et al.* [1972] and *Yoon et al.* [1992].The validity of this approach requires that the bandwidth of the excited fluctuations defines a range of resonant velocities comparable to or larger than the thermal velocity of the resonant component. In such cases the plasma evolves through changes in the moments of the components (j) including the drift velocity (v_{0j}), and the parallel ($T_{||j}$) and perpendicular ($T_{\perp j}$) temperatures. Furthermore, since the anisotropy instability provides maximum growth for waves with phase velocities aligned along $\mathbf{B}_0$ [*Gary, 1993*], it is assumed that $\mathbf{k}\times\mathbf{B}_0=0$. Under these constraints and the usual assumptions associated with the quasi-linear approach [*Galeev and Sagdeev*, 1983] it can be written

$$\frac{\partial}{\partial t}p_{||j}(t) = n_j m_j \frac{\partial}{\partial t}v_{0j}(t) = \frac{\omega_j^2}{c^2}\sum_\alpha \int_0^\infty dk_{||} \sum_{+,-} \frac{\xi^{\pm B_1}_{k,\alpha}(t)}{k_{||}^2}\frac{|\omega^\pm|^2}{\omega^\pm \omega^\mp} \cdot \left[\left(\frac{i\omega^\pm + ik_{||}v_{0j}(t)}{k_{||}v_j}\right)Z\left(\zeta_j^\pm\right) - i\left(1-\frac{T_{\perp j}(t)}{T_{||j}(t)}\right)\frac{Z'\left(\zeta_j^\pm\right)}{2}\right], \quad (1)$$

$$n_j\frac{\partial}{\partial t}T_{||j}(t) = \frac{\omega_j^2}{c^2}\sum_\alpha \int_0^\infty dk_{||} \sum_{+,-} \frac{\xi^{\pm B_1}_{k,\alpha}(t)}{k_{||}^2}\frac{|\omega^\pm|^2}{\omega^\pm \omega^\mp} \cdot \left[\left(\frac{\omega^\mp v_{0j}(t) - \omega^\pm v_{0j}(t) - i\left((\omega^\mp\omega^\pm)/k_{||}\right) + ik_{||}v_{0j}^2(t)}{k_{||}v_j}\right)Z\left(\zeta_j^\pm\right) - \left(\frac{\omega^\mp - \omega^\pm - \frac{T_{\perp j}(t)}{T_{||j}(t)}\left(\omega^\mp - ik_{||}v_{0j}(t)\right) - 2ik_{||}v_{0j}(t)}{k_{||}} - i\zeta_j^\pm v_j\left(1-\frac{T_{\perp j}(t)}{T_{||j}(t)}\right)\right)\frac{Z'\left(\zeta_j^\pm\right)}{2}\right], \quad (2)$$

$$n_j\frac{\partial}{\partial t}T_{||j}(t) = \frac{\omega_j^2}{c^2}\sum_\alpha \int_0^\infty dk_{||} \sum_{+,-} \frac{\xi^{\pm B_1}_{k,\alpha}(t)}{k_{||}^2}\frac{|\omega^\pm|^2}{\omega^\pm \omega^\mp} \cdot \left[v_j\left(-i\zeta_j^\pm\left(1-\frac{T_{\perp j}(t)}{T_{||j}(t)}\right) - \left(\frac{\omega^\pm + ik_{||}v_{0j}(t)}{k_{||}v_j}\right)\right)\frac{Z'\left(\zeta_j^\pm\right)}{2}\right], \quad (3)$$

where $\xi^{\pm B_1}_{k,\alpha}$ is the spectral energy density of the magnetic field fluctuations of wave mode α, $\omega^+=\omega_k{}^+(t)+i\gamma k^+(t)$ and $\omega^-=\omega_k{}^-(t)+i\gamma_k{}^-(t)$ are the positive and negative helicity solutions of the electromagnetic dispersion relation, $D(\omega,k)=0$ [*Gary*, 1993] at time t and wavenumber k, ω_j is the plasma frequency ($\omega_j=(4\pi n_e q_j{}^2/m_j)^{1/2}$), v_A is the Alfven speed ($v_A=B_0/(4\pi n_e m_p)^{1/2}$), $\beta_{\perp c}$ is plasma beta for the proton core ($\beta_{\perp c}=8\pi n_e T_{\perp c}/B_0{}^2$), v_j is the thermal velocity ($v_j=2T_{\perp j}/m_j$) and $\zeta_j{}^\pm=(\omega-k_{||}v_{0j}\pm\Omega_j)/k_{||}v_j$. $\xi^{\pm B_1}_{k,\alpha}$ is related to the spectral energy density of the electric field fluctuations, $\xi^\pm_{k,\alpha}$, through Faraday's law, $\xi^{\pm B_1}_{k,\alpha} = \xi^\pm_{k,\alpha}c^2k_{||}^2/|\omega^\pm|^2$. These equations together with the electromagnetic dispersion relation [Gary, 1993] and the relationship between spectral energy density $\xi^\pm_{k,\alpha}$ and $\gamma_k(t)$,

$$\frac{\partial}{\partial t}\xi^\pm_{k,\alpha}(t) = 2\gamma^\pm_{k,\alpha}\xi^\pm_{k,\alpha}(t), \quad (4)$$

form a complete self-consistent set describing the evolution of a weakly turbulent plasma under the usual quasi-linear constraints and where the density is invariant with time and the drift velocity perpendicular to B_0 of any component is zero. A more detailed discussion of the derivation of these equations can be found in the work of *Chaston et al.* [1999b].

3. Ion Cyclotron Heating in the Central Plasma Sheet

Using (1)-(4) the evolution of a plasma containing the species H^+, O^+, He^+, and He^{++} and e^- and representing distributions in the central plasma sheet is studied. Two sets of parameters are examined and are labeled A and B in Table 1. The proton and electron temperatures are consistent with typical quiet time plasma sheet observations. In the case of the heavy ion components, particularly He^+ and O^+ the initial temperatures are typical of the polar wind to investigate the possibility of local heavy ion heating to temperatures closer to those found by insitu observations. For the five-component plasma considered, four Alfvenic roots of the dispersion relation [*Gary*, 1993] occur each bounded above by a resonance with one of the ion species and below by a cutoff above a narrow stopband [*Chaston et al.*, 1997]. For brevity we label each

Table 1. Normalized Initial Moment Parameters for Two (A,B) Central Plasma Sheet Simulations.

Species	n_j/n_t		$T_{\perp j}/T_{\perp c}$		$T_{\perp j}/T_{\|\|j}$
	A	B	A	B	
H^+	0.88	0.8	1.0	1.0	2.5
He^+	0.01	0.05	0.002	0.01	1.0
He^{++}	0.01	0.05	0.002	0.01	1.0
O^+	0.1	0.1	0.002	0.01	1.0
e^-	1.01	1.01	0.1	0.1	1.0

Assuming a background field strength of 15 nT these parameters correspond to a total ion density of 0.3 cm^{-3} and $T_{\perp c}$=7.5 keV. Here $\beta_{\perp c}$=4.0, $v_{A(H+)}/c$=0.002

of these roots starting with the lowest-frequency mode the O^+, He^+, He^{++}, and H^+ branches.

In each simulation the initial wave energy density is considered uniform over the range of unstable wavenumbers and has value 0.0001 $n_i T_{\perp c}$. For the parameters given in Table 1 this wave energy density is equivalent to $(B_1/B_0)^2=4.02\text{x}10^{-6}$ or an initial wave amplitude of 0.03 nT for all unstable wavenumbers. It should be noted that since all components have zero drift the dispersion results ($D(\omega,k)=0$) are symmetric with respect to $\mathbf{k}$ such that $\gamma_k^+=\gamma_k^-$ and $\omega_k^+=-\omega_k^-$. As a result, it is only necessary to discuss the dispersion results for one helicity. Here we consider the negative helicity results (ω_k^-,γ_k^-).

Figure 1a shows the temporal variation of real frequency and growth rate for case study A. At $t\Omega_p=0$ the anisotropy instability occurs on both the H^+ and He^+ Alfven branches with maximum growth at $\omega/\Omega_p\sim0.5$ where the two branches become coupled. At later times during the simulation the frequency of maximum growth falls to increasingly lower values and the instability becomes isolated to the He^{++} branch except for negligible growth on the He^+ branch (not shown) at $t\Omega_p\geq60$. The falling growth rate shown in Figure 1b is reflected in the decreasing anisotropy of the proton component shown in Figure 2 with linear saturation of the instability after $t\Omega_p\sim80$ (or ~56 s if B_0=15 nT).

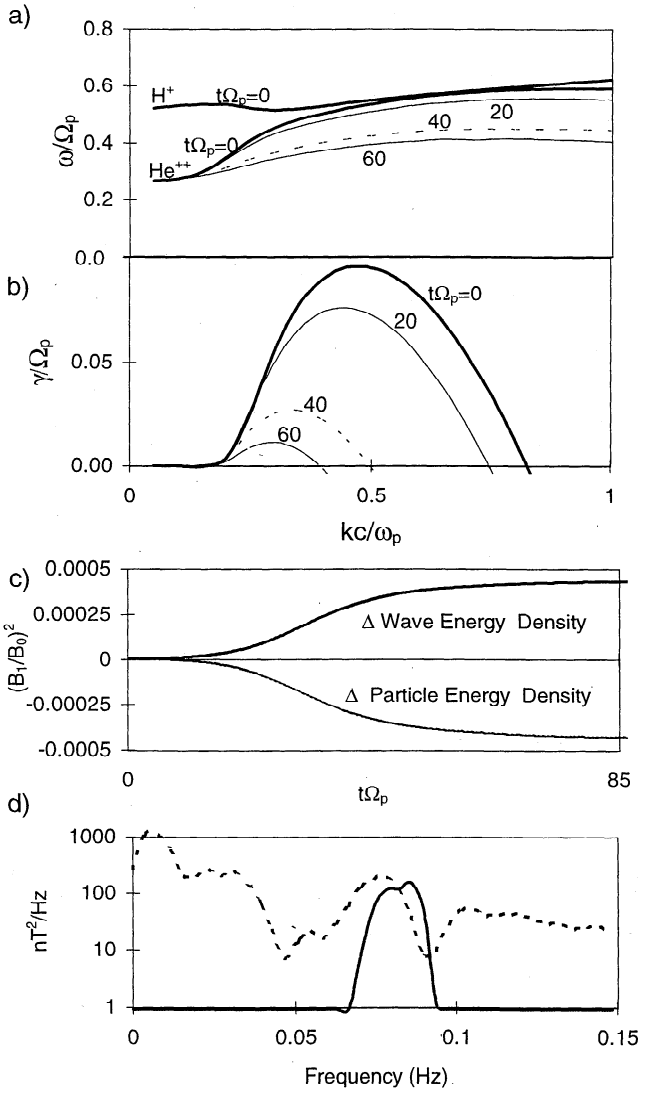

Figure 1. Variations in wave properties during the evolution of the plasma sheet model A. (a) Changes in the wave dispersion of the He^{++} branch at $t\Omega_p$=0, 20, 40, 60. (b) Changes in growth rate for the proton anisotropy instability at the same times. (c) Increase in total wave energy and equal decrease in total particle energy over the time required to saturate the anisotropy instability. (d) Magnetic wave spectrum at the time of saturation; the solid line is the simulation result, while the dashed line is the observed wave spectrum averaged over the interval 1978-04-02/1855-56 UT.

Coincident with the saturation of the instability is the increase in the spectral energy density of the magnetic field fluctuations. As indicated in Figure 1c, the increase in wave energy density is matched by the energy loss in the particles. The average wave amplitude for the chosen parameters is 0.33 nT with a peak of 0.49 nT at kc/ω_p=0.4 and ω/Ω_p=0.38. Figure 1d shows the saturated quasi-linear magnetic field wave spectrum. The wave is narrow banded in this case and matches a peak in the observed wave spectrum for a central plasma sheet ion cyclotron wave event reported by *Chaston et al.* [1999a] which is represented in Figure 1d by the dashed line.

Saturation of the anisotropy instability is achieved through energy isotropization so that $T_{\perp j}/T_{\|j} \leq \Omega_i/(\Omega_i-\omega_r)$ [*Kennel and Petschek*, 1966]. It is this process which provides the free energy necessary for wave growth. Figure 2 shows the temperature evolution for each ion species present in the simulation. The curves for the unstable proton component (first row) show that the reduction in anisotropy is achieved through a large increase (50%) in $T_{\|p}$ and a small (10%) reduction in $T_{\perp p}$. Saturation occurs with $T_{\perp j}/T_{\|j}$ =~1.6.

The second row of Figure 2 shows that for O^+ ions, $\Delta T_\|$ is negligible and $T_\perp(t)/T_\perp(0)\sim4$ at the time of saturation ($\Delta T_\perp$=45 eV for the parameters suggested above). The He^+ ions (third row, Figure 2) are strongly heated with $T_\|(t)/T_\|(0)$=45 and $T_\perp(t)/T_\perp(0)$=140 at saturation. Since the initial rate of change in $T_\perp$ is larger than in $T_\|$, the anisotropy of this species increases rapidly and in fact becomes unstable to the anisotropy instability itself. This effectively slows the rate of perpendicular heating so that the anisotropy of He^+ remains at the instability threshold throughout the remainder of the simulation. Note also how the He^+ heating continues at the same rate toward saturation. For the typical parameters suggested above, the final temperatures of this component are $T_\|$=675 eV and $T_\perp$=2100 eV. The He^{++} ions (fourth row, Figure 2) also exhibit a peak in anisotropy at which time the distribution becomes marginally unstable thereby reducing the perpendicular heating rate throughout the remainder of the simulation. These ions are efficiently heated with $T_\|(t)/T_\|(0)$=130 and $T_\perp(t)/T_\perp(0)$=425 before saturation corresponding to final temperatures of $T_\|$=1950 eV and $T_\perp$=6375 eV.

In case study B (the lighter curves in Figure 1) the simulation is begun with higher heavy ion temperatures and densities. Since the total energy made available through isotropization of the proton distribution remains basically the same, the amount of heating experienced by the heavier ions is reduced significantly. In fact, the energy gain is approximately inversely proportional to the increase in density for each heavy ion species. For the He^{++} ions in B the initial temperature has been increased to a value more representative of temperatures found for this species in the solar wind. Nonetheless, a several fold increase in the temperature still occurs.

4. Ion Cyclotron Heating in the Plasma Sheet Boundary Layer

In the plasma sheet boundary layer the streaming of the unstable anisotropic population causes a large Doppler shift of the ion cyclotron wave in the rest frame. Consequently, the unstable wave

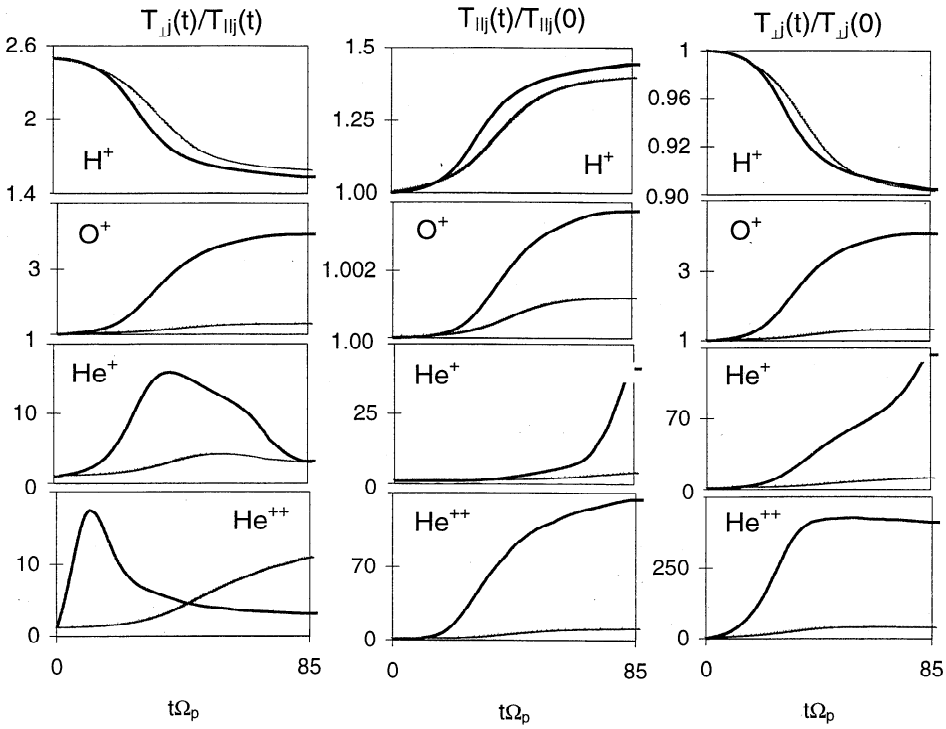

Figure 2. Changes in temperature for each ion species over the saturation time for the central plasma sheet models given in Table 1. The darker and lighter curves are the solutions for model A and B, respectively. The first column presents the time rate change in temperature anisotropy, $T_\perp/T_\parallel$. The second column shows the variation in parallel temperature, $T_\parallel(t)$, normalized in terms of the initial parallel temperature, $T_\parallel(0)$. The third column shows the variation in perpendicular temperature, $T_\perp(t)$, normalized in terms of the initial perpendicular temperature, $T_\perp(0)$.

frequencies may extend across the resonances of the different ion species as has been shown by *Chaston et al.* [1999a]. This can complicate the numerical study of the anisotropy instability particularly when the plasma carries a current. To simplify the problem, we consider a currentless plasma. For the nonzero current case we refer the interested reader to *Chaston et al.* [1999b] where the current-driven instability is studied in a drifting anisotropic proton-electron plasma.

Again, two sets of initial parameters are employed as indicated in Table 2. Both represent the quiet time plasma sheet boundary layer and include a cool proton core, two counterstreaming anisotropic proton beams and cool O^+, He^+, and He^{++} distributions. It is assumed that the initial (background) wave energy is uniform over all unstable wavenumbers with value $0.01 n_t T_{\perp c}$, which corresponds to B_1=0.02nT or $(B_1/B_0)^2$=6.43x10^{-7} if B_0=25 nT.

Since the proton beams are of equal density but opposite drift velocity along B_0, here again the positive and negative helicity solutions of $D(\omega,k)$=0 are symmetric. Figures 3a-3d are snapshots of the negative helicity real-frequency dispersion curves for the He^{++}, He^+, and O^+ branches at $t\Omega_p$=0, 30, 60, 120. Extrapolating from the growth rate curves of Figure 3e onto the real frequency curves of Figures 3a-3d shows that because of the mode coupling that the Doppler shift provides, instability occurs on all three branches along the Doppler-shifted portion of each curve. As the growth rate decreases in time, the range of unstable wavenumbers contracts (and hence also the frequency range) until positive growth occurs on the He^+ branch alone before saturation. Figure 3f shows the change in particle and wave energy throughout the evolution of the system. For a background field of 25 nT the saturated wave amplitude is 0.32 nT. The saturated wave spectrum shown in Figure 3g is broadband and similar to that observed during a plasma sheet boundary later crossing studied by *Chaston et al.* [1994] and presented here by the dashed line in this panel.

Figure 4 shows the temperature variation of each component. The first row shows small nonresonant heating of the core protons in the perpendicular direction. The saturation of the instability occurs in the same manner as discussed in the previous section for the central plasma sheet anisotropy instability. The second row of Figure 4 indicates a final proton beam anisotropy of ~3.2. There is almost no change in the proton beam velocity except for a negligible decrease representing ~1/40 of the total energy lost from the particles. For this reason the beam velocity variation curves have been omitted.

For the heavy ions a similar pattern to that occurring in the central plasma sheet emerges. The O^+ component is heated slightly in the perpendicular direction with an increase from 10 to 33 eV. The He^+ ions experience strong heating with $T_\parallel(t)/T_\parallel(0)$=30 and $T_\perp(t)/T_\perp(0)$=345 before saturation corresponding to final temperatures of $T_\parallel$=300 eV and $T_\perp$=3450 eV. Again, notice that the heating continues at the same rate even though the instability is very close to stable after $t\Omega_p$=180. Importantly, at times following $t\Omega_p$=40 the anisotropy of the He^+ ions is sufficient to excite the He^+ ion anisotropy instability. This instability does not appear on the Doppler-shifted portions of the real frequency curves but rather occurs close to the He^+ resonance. Its growth rate throughout the remainder of the simulation remains too small to be visible in Figure 3e. The effect of this instability has not been included in the quasi-linear analysis. However, since the magnitude of the growth rate at any

Table 2. Normalized Initial Moment Parameters for Two (A,B) Plasma Sheet Boundary Layer Simulations.

Species	n_j/n_t		$T_{\perp j}/T_{\perp c}$		$T_{\perp j}/T_{\parallel j}$	v_{oj}/v_A
	A	B	A	B		
H^+ Core	0.08	0.02	1.0	1.0	1.0	0.0
H^+ Beam	0.4	0.4	50	50	8	0.6
H^+ Beam	0.4	0.4	50	50	8	-0.6
He^+	0.01	0.04	0.1	1.0	1.0	0.0
He^{++}	0.01	0.04	0.1	10	1.0	0.0
O^+	0.1	0.1	0.1	1.0	1.0	0.0
e^-	1.01	1.04	1.0	1.0	1.0	0.0

Assuming a background field strength of 25 nT these parameters correspond to a total ion density of 0.1 cm^{-3} and $T_{\perp c}$=100 eV. Here $\beta_{\perp c}$=0.0064, and $v_{A(H+)}/c$=0.0058.

time is at most 1/10th of maximum growth rate of the Doppler-shifted instability we consider its importance as secondary. Furthermore, the Doppler-shifted instability acts in the same way upon the He^+ anisotropy as attested by the decreasing anisotropy of these ions subsequent to $t\Omega_p$=40.

For the parameters of model B the increased density of the heavy ion components tends to decouple the dispersion curves as the heating process proceeds. This separates the instability into two peaks on the Doppler-shifted portions of the He^{++} and He^+ branches so that now a stopband exists between the growing waves on each branch. The obvious affect of increasing the density of heavy ion species is a decrease in the temperature change which as in the central plasma sheet case is roughly inversely proportional to the increase in heavy ion density. Final temperatures of He^{++} in this case are $T_\perp$=1250 and $T_\parallel$=880 eV.

5. Discussion

5.1. Resonant and Nonresonant Heating

The ion heating results can be understood in terms of the cyclotron resonant and nonresonant interaction of the ions with the growing wave field. The resonance condition may be expressed in a normalized form as

$$\bar{\zeta}_j^{\pm} = \sqrt{\frac{(T_{\perp j}/T_{\parallel j})}{\beta_{\perp c}(T_{\perp j}/T_{\perp c})}\frac{m_j}{m_c}}\left(\frac{\omega_o}{k_o} - \frac{v_{oj}}{v_A} \pm \frac{q_j}{q_c}\frac{m_c}{m_j}\frac{1}{k_o}\right), \quad (5)$$

where $k_o=kc/\omega_p$ and $\omega_o=\omega/\Omega_p$ are the normalized wavenumber and wave frequency. The component j may be considered resonant if $\bar{\zeta}_j^- \le 1$, weakly resonant if $\bar{\zeta}_j^- > 1$, and nonresonant if $\bar{\zeta}_j^- >> 1$. Figure 5 shows the variation in heating rate and $1/\bar{\zeta}_j^-$ with t. T_j is the sum of the perpendicular and parallel temperatures in eV. Values of $1/\bar{\zeta}_j^- \ge 1$ indicate strong resonance. For the O^+ ions in the central plasma sheet case study, $1/\bar{\zeta}_j^-$ remains less than 0.1 throughout. Consequently, this species is nonresonant and is only slowly

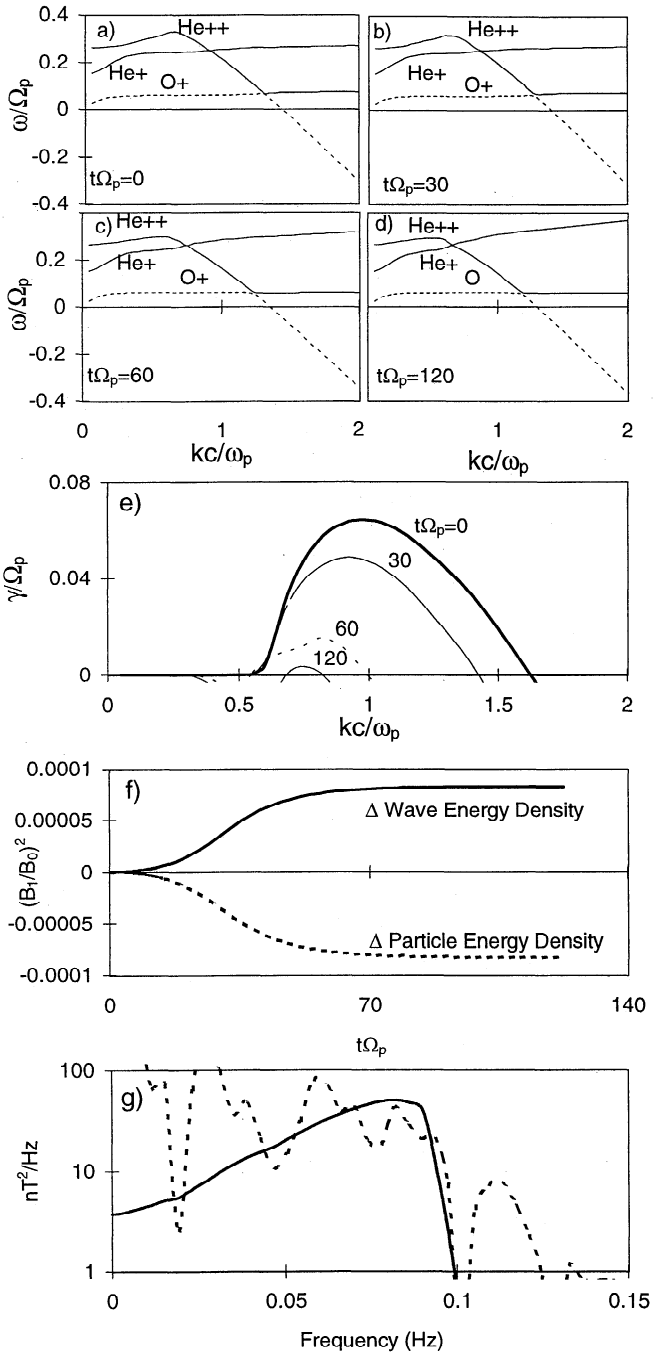

Figure 3. Variations in wave properties during the evolution of the plasma sheet boundary layer model A. (a-d) Changes in the wave dispersion of the He^{++}, He^+, and O^+ branches at $t\Omega_p$=0, 30, 60, and 120. The instability occurs on the Doppler shift portions of these curves. (e) Changes in growth rate for the proton beam-anisotropy instability at the same times. (f) Increase in total wave energy and equal decrease in total particle energy over the time required to saturate the anisotropy instability. (g) Magnetic wave spectrum at the time of saturation; the solid line is the simulation result, while the dashed line is the observed wave spectrum averaged over the interval 1978-04-18/0923-24 UT.

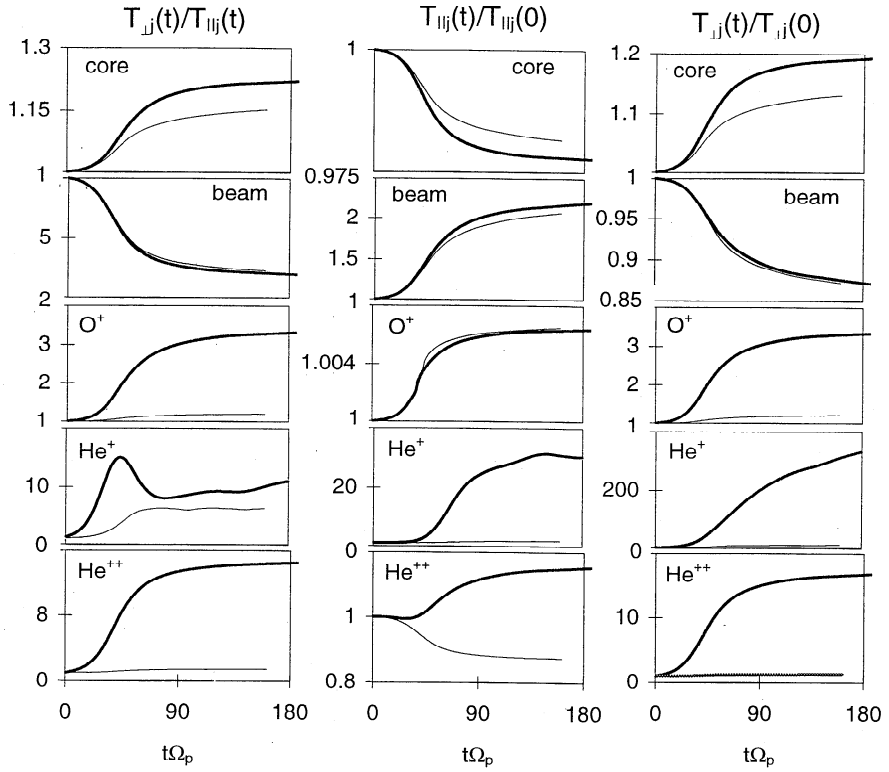

Figure 4. Changes in temperature for each ion species over the saturation time for the plasma sheet boundary layer models given in Table 2. The darker and lighter curves are the solutions for model A and B, respectively. The first column presents the time rate change in temperature anisotropy, $T_\perp/T_\parallel$. The second column shows the variation in parallel temperature, $T_\parallel(t)$, normalized in terms of the initial parallel temperature, $T_\parallel(0)$. The third column shows the variation in perpendicular temperature, $T_\perp(t)$, normalized in terms of the initial perpendicular temperature, $T_\perp(0)$.

"heated" in the perpendicular direction due to the $\mathbf{E}_1\times\mathbf{B}_0$ drift of each ions guiding center in the growing wave field [*Chaston et al.*, 1999b]. The nonresonant heating process as modeled does not really represent a change in the temperature of the distribution function since it is isentropic. As discussed by *Krall and Trivelpece* [1973] and *Gary et al.* [1995, 1996a], the process is reversible so that the component will return to its original temperature if the wave field is removed. A similar explanation can be extended to account for O^+ heating in the central plasma sheet. However, it seems reasonable to include these variations as temperature changes from an observational perspective since the integration time of spacecraft borne electrostatic analysers averages the distribution over times longer than the observed wave period.

For the He^+ ions in both the central plasma sheet and boundary layer a two-stage heating process occurs. As indicated by the curves in Figure 5, this species is initially nonresonant with the growing wave and the heating rate is small. However, as the instability approaches saturation, the bandwidth for wave growth in both the central plasma sheet and plasma sheet boundary layer shifts to lower frequencies. This combined with slight nonresonant heating brings an ever increasing fraction of the He^+ ions into resonance with the growing wave field and so the heating rate increases. Effectively, the combined influence of the increasing thermal velocity of the He^+ distribution and the falling wave frequency of the instability with decreasing proton anisotropy brings the He^+ ions into resonance so that rapid heating results after $t\Omega_p$~70 (~50 s) in the central plasma sheet case and after $t\Omega_p$~50 (~20 s) in the boundary layer. This occurs despite the significantly decreased growth rate of the instability at these times from its value at $t\Omega_p$=0. In fact, as indicated earlier, in the central plasma sheet case the He^+ heating rate increases until saturation of the proton anisotropy instability and continues after this time and in the plasma sheet boundary layer heating continues beyond the saturation time when the simulation was stopped. Consequently, the final temperature of this species is uncertain but is certainly larger than the final temperatures reported above. *Gary et al.* [1995, 1996a] comments on the same effect for cool He^+ heating determined from hybrid simulations for the proton anisotropy instability in the outer magnetosphere and indicates that this result is consistent with the predictions a simplified quasi-linear or second-order approach [*Gary and Tokar*, 1985]. Essentially, this shows that in the presence of broadband field fluctuations covering the frequencies resonant with He^+ ions, heating of this species proceeds and does so without the need for local plasma instability.

For the He^{++} ions in the central plasma sheet and plasma sheet boundary layer the heating mechanisms responsible differ. The central plasma sheet He^{++} ions are strongly resonant with the growing wave particularly at wavenumbers close to the coupling between the H^+ and He^{++} branches until $t\Omega p$~60 (~ 40 s). In fact, at $t\Omega_p$~15 (~10 s), $1/\overline{\zeta}^-=1/\overline{\zeta}^+\Rightarrow\infty$ at the wavenumber of maximum growth. As a result, these ions have a large heating rate throughout the simulation until saturation of the proton anisotropy instability. The value of $T_{\perp He++}/T_{\parallel He++}$ is limited by the condition of marginal instability to the He^{++} anisotropy instability. For this reason, $T_{\perp He++}$ actually decreases slightly after $t\Omega_p$=40 or (28 s), while $T_{\parallel He++}$ continues to increase. This species, however, becomes less

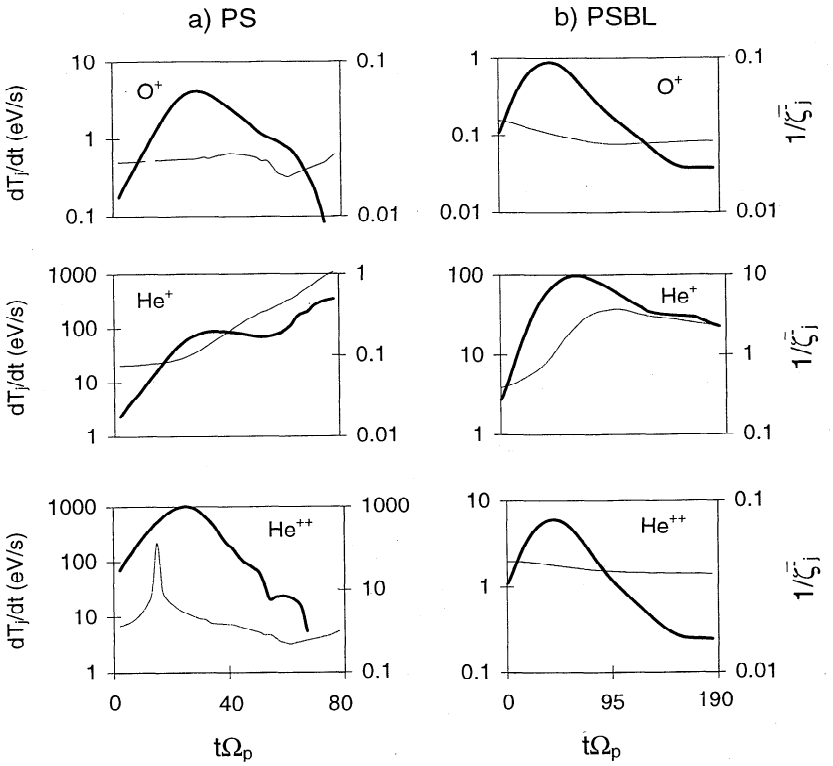

Figure 5. Heating rates (on the primary y axis) and resonance conditions (on the secondary y axis) for the (a) the central plasma sheet and (b) the plasma sheet boundary layer using the simulation results from model A in each case. The darker curves represent the ion heating rate, dT_j/dt, while the lighter curves are the inverse value of the resonance condition, $1/\bar{\zeta}_j$, given by (5) at the frequency and wavenumber of maximum wave growth at the normalized time, $t\Omega_p$. Here $T_j=T_{\perp j}(t)+T_{\|j}(t)$ in eV.

resonant as the system evolves and heating rates fall toward zero as the anisotropy instability saturates. In the plasma sheet boundary layer, Figure 5 shows that the He^{++} ions are nonresonant throughout and so have slower heating rates.

5.2. Comparison to Hybrid Simulations

A simple test of the veracity of the results obtained by this technique is direct comparison to those obtained from full simulations. An obvious potential shortcoming of quasi-linear approach adopted here is the assumption that the distributions maintain bi-Maxwellian form throughout the simulation. The hybrid simulations of [*Gary et al.*, 1996b] show that the functional form of an anisotropic proton distribution does in fact remain bi-Maxwellian as the anisotropy is relaxed through proton cyclotron wave emission. Further, for drifting anisotropic components unstable to the beam-anisotropy instability the hybrid simulations of *Gary and Winske* [1990] show that ion beam distributions are weakly pitch angle scattered with a net decrease in temperature anisotropy associated with the instability saturation. Consequently, for the anisotropy instability under consideration here, the evolution of the plasma can be studied approximately in terms of the variation in the velocity moments including the drift velocity ($v_{0j}(t)$), and perpendicular ($T_{\perp j}(t)$) and parallel ($T_{\| j}(t)$) temperature of each component in the plasma.

The random phase approximation invoked in the quasi-linear technique removes any phase specific mechanisms such as phase bunching or trapping which are included in the hybrid approach. The effect of such processes is usually to saturate the instability before linear stability is reached. *Gary and Winske* [1990] have performed hybrid proton-electron simulations for plasma sheet boundary layer distributions similar to that adopted for the quasi-linear PSBL case studied here. These results can be compared directly to the quasi-linear results. In agreement we find $(B_1/B_0)^2 << 1$, however, our saturation time is of the order of 50% longer than found in the full simulation in which stability is attained after $t\Omega_p$ =100. In addition, for the quasi-linear results the plasma becomes stable with a beam anisotropy of ~3.2 at saturation which is somewhat lower than the 4.8 predicted from simulations. In fact, at saturation the plasma in the hybrid simulation is still linearly unstable. This suggests that the shorter saturation time and the larger beam anisotropy at saturation are likely the result of wave trapping. Nonetheless, considering that *Gary and Winske* [1990] use larger beam temperatures, beam anisotropies B_0, smaller beam velocities, and do not include a cold stationary ion component or the effects of heavy ions, the results are basically in reasonable agreement with the damping effects of wave trapping becoming more important towards the end of the simulation.

Hybrid codes have also been employed to examine the heating of He^+ ions by waves grown from the anisotropy instability in the dayside equatorial magnetosphere [*Tanaka*, 1985; *Omura et al.*, 1985; *Machida et al.*, 1988] and magnetosheath [*Gary et al.*, 1996a]. While these simulations have been performed for somewhat different plasmas than considered in this study the heating process is similar. Consistent with the quasi-linear heating rates presented in Figure 5, it is shown [*Gary et al.*, 1996a] that the maximum heating rate coincides with the time of strongest resonance

for the He^+ ions. Furthermore, in the hybrid simulations this species is initially reversibly heated as the ions oscillate in the wave field in a manner analogous to the quasi-linear case where He^+ ions are initially nonresonantly accelerated as $\mathbf{E}_1 \times \mathbf{B}_0$ increases with $\mathbf{E}_1$. The transition from nonresonant to resonant interaction with the growing wave field and the corresponding increase in heating rate is apparent in both techniques. *Omura et al.* [1985] and *Gary et al.*, [1996a] obtain He^+ anisotropies with a similar profile to the quasi-linear results given in Figures 2 and 4, where initially larger heating is observed in the perpendicular direction providing a peak in $T_{\perp He+}/T_{\|He+}$ followed by partial isotropization as the parallel heating rate increases at later times.

5.3. Comparison With Heavy Ion Energy Observations

Since the saturation time of the instability (2 min) is several times less than the time resolution of the mass spectrometer ion moment data available (13 min) from the ISEE mission, a detailed comparison between the time evolution of observed and predicted ion temperatures is not possible and a statistical study of ion temperatures in the near-Earth magnetotail goes beyond the scope of this work. For these reasons we will discuss observed mass specific energy results covering two MNBs, one in the central plasma sheet [*Chaston et al.*, 1999a] and a second in the plasma sheet boundary layer [*Chaston et al.*, 1994]. The magnetic field spectra for each of these appear in Figures 1d and 3g.

For the central plasma sheet ion cyclotron wave event (1978-04-02/1850 UT), the moment data show that there is a peak in energy for the He^+ and He^{++} ions at the time of the wave event with perpendicular energies of 4700 and 9150 eV and parallel energies of 2290 and 5110 keV respectively averaged over the interval from 1978-04-02/1846-59 UT. In the absence of significant perpendicular drifts and taking into account the parallel drift, these energies suggest $T_\perp$~2350 eV, $T_\perp$~4550 eV, and $T_\|$=2070 eV and $T_\|$=4900 eV for He^+ and He^{++} ions, respectively, which is similar to the modeled results at saturation of the instability ($T_\perp$=6375 He^{++}, 2100 He^+, 60 O^+ eV; $T_\|$=1950 He^{++}, 675 He^+, 15 O^+ eV) albeit somewhat more isotropic. The O^+ ions, however, are significantly hotter than predicted with $T_\perp$ ~2200 eV. In the case of the plasma sheet boundary layer MNB (1978-04-18/0923 UT) the approximate observed temperatures based on moment values in the limit of no perpendicular drift are $T_\perp$~3100, 1650 and 1090 eV and $T_\|$~6400, 748 and 296 eV for He^{++}, He^+ and O^+ ions respectively. These temperatures are larger than predicted ($T_\perp$=1250 He^{++}, 3450 He^+, 33 O^+ eV; $T_\|$=880 He^{++}, 300 He^+, 10 O^+ eV) except in the case of He+ where a lower final temperature than predicted is obtained.

The modeling results provide at least an order of magnitude estimate for the temperatures of He^{++} and He^+ in this region of space. Considering that the initial temperature of each component is unknown and the fact that each species may have undergone several heating events prior to its interaction with the individual MNBs makes an accurate case study analysis difficult and predicted temperatures can be expected to be less than those observed. For O^+ ions however the modeled temperature is too low. As indicated in Figures 1d and 3g, observations of MNBs exhibit significantly larger spectral energy densities below 50 mHz than the modeling predicts. Significantly, this range contains the O^+ gyrofrequency. *Chaston et al.* [1999b] has shown that these energy densities may be partially due to the contribution from current driven instability which grows to spectral energy densities equivalent to the anisotropy instability. As mentioned earlier, for the sake of simplicity this contribution has been ignored in this study. Enhancing the modeled spectrum at frequencies of the order of the O^+ gyrofrequency by inclusion of these instabilities may be sufficient to account for observed O^+ temperatures in the keV range.

6. Conclusion

Ionospheric ions arriving in the central plasma sheet and its boundary layer whether as part of the polar wind or from the auroral oval should be closely field-aligned. However, the results presented by *Lennartsson et al.* [1985] indicate that typically these ions have broad pitch angle and energy spectra. This work provides a possible explanation for the velocity distribution of these ions motivated by observation of broadband magnetic noise (MNBs) [*Bauer et al.*, 1995] and linearly unstable hot proton distributions in these regions [*Angelopoulos et al.*, 1989; *Chaston et al.*, 1999a].

For a plasma initially unstable to the proton anisotropy instability and typical of the central plasma sheet and boundary layer we have performed quasi-linear simulations to self-consistently follow the evolution of the wave spectra and plasma moments as the system saturates. In this way He^+ ions have been shown to be heated via a two-step nonresonant to resonant process from 10 eV up to >3 keV. O^+ ions experience nonresonant heating from 10 eV up to ~100 eV. This temperature change is, however, reversible and dependent on the local wave amplitude. He^{++} ions are weakly heated in the plasma sheet boundary layer but experience strong heating in the central plasma sheet. Final temperatures for this species are of the order of 7 keV consistent with the observations of *Lennartsson et al.*, [1985] who show enhanced He^{++} energies in the plasma sheet and those of *Lennartsson and Shelley* [1986] who show that the energy of this species is lowest in the flanks of the plasma sheet and increases toward the central axis $Y_{GSM}=Z_{GSM}=0$. These authors also discuss the inverse relationship between the density and thermal energy of this species which is suggestive of the modeling performed where due to the overall energy budget the more dense the He^{++} (or ionospheric) ions the lower their temperature.

In terms of wave properties similar wave amplitudes (≤1 nT) or spectral densities and polarization to that reported by *Chaston et al.* [1999a] are obtained and at least a portion of the magnetic wave spectrum can be explained in this manner. Inclusion of current driven instability improves the comparison between modeled and observed spectral results and may push the temperature of O^+ ions above 1keV [*Chaston et al.*, 1999b].

In conclusion, this study emphasizes that the observed ionospheric and solar wind ion distributions observed from the ISEE spacecraft in the near-Earth magnetotail may be a result of local heating due to interaction with the MNBs prevalent in these regions. This does not imply that it is the only process contributing to the temperatures of heavy ions seen in these regions but rather is perhaps an important factor in the evolution of ion distributions as they stream antisunward from the high latitude ionosphere or enter the plasma sheet from the magnetosheath. In fact, observations show that ion waves occur almost continually along the entire length of fieldlines emanating from the high-latitude ionosphere and into the magnetotail. Observations in the auroral oval of ion cyclotron waves are numerous [*Kintner et al.*, 1979; *Temerin and Lysak*, 1984; *Andre et al.*, 1998; *Cattell et al.*, 1998; *Erlandson and Zanetti*, 1998; *Lund et al.*, 1998] and several theoretical studies have shown how such waves may lead to the heating of ionospheric ions [*Andre and Yau*, 1997]. At higher altitudes, *Mozer et al.* [1997] reports the presence of ion cyclotron waves from the

Polar spacecraft. *Bauer et al.* [1995] and *Chaston et al.* [1999a] have presented statistical studies of waves close to ion cyclotron frequencies in the near-Earth magnetotail and *Tsurutani et al.*, [1985] has reported the existence of such waves in the distant magnetotail. This suggests a scenario whereby ions maybe continually heated as they stream tailward from the ionosphere (in the case of ionospheric ions) or near-Earth plasma sheet (in the case of solar wind ions) and become resonant (or to a lesser extent nonresonant) with the ion waves occurring along their paths.

Acknowledgments. This research was supported by grants from the Australian Research Council, The University of Newcastle and NASA (NAG5-3596). The authors express their gratitude to NSSDC for supplying the Lockheed Mass Spectrometer data from the ISEE spacecraft used in this study.

Hiroshi Matsumoto thanks T. E. Eastman and Y. Saito for their assistance in evaluating this paper.

References

Akimoto, K., and N. Omidi, The generation of broadband electrostatic noise by an ion beam in the magnetotail, *Geophys. Res. Lett., 13*, 97, 1986.

Andre, M., and A. W. Yau, Theories and observations of ion energisation and outflows in the high latitude magnetosphere, *Space Sci. Rev., 80*, 27, 1997.

Andre, M., P. Norqvist, L. Andersson, L. Eliasson, A. I. Eriksson, L. Blomberg, R. E. Erlandson, and J. Waldemark, Ion energization mechanisms at 1700 km in the auroral region, *J. Geophys. Res., 103*, 4199, 1998.

Angelopoulos, V., R. C. Elphic, S. P. Gary, and C. Y. Huang, Electromagnetic instabilities in the plasma sheet boundary layer, *J. Geophys. Res., 94*, 15,373, 1989.

Ashour-Abdalla, M., L. A. Frank, W. R. Paterson, V. Peroomian, and L. M. Zelenyi, Proton velocity distributions in the magnetotail: Theory and observations, *J. Geophys. Res., 101*, 2587, 1996.

Bame, S. J., J. R. Asbridge, H. E. Felthauser, E. W. Hones, and I. B. Strong, Characteristics of the plasma sheet in the Earth's magnetotail, *J. Geophys. Res., 72*, 113, 1967.

Bauer, T. M., W. Baumjohann, R. A. Treumann, N. Sckopke, and H. Luhr, Low-frequency waves in the near-Earth plasma sheet, *J. Geophys. Res., 100*, 9605, 1995.

Cattell, C., *et al.*, The association of electrostatic ion cyclotron waves, ion and electron beams and field-aligned currents: FAST observations of an auroral zone crossing near midnight, *Geophys. Res. Lett., 25*, 2053, 1998.

Chaston, C. C., Y. D. Hu, B. J. Fraser, R. C. Elphic, and C. Y. Huang, Electromagnetic ion cyclotron waves observed in the near-Earth plasma sheet boundary layer, *J. Geomagn. Geoelectr., 46*, 987, 1994.

Chaston, C. C., Y. D. Hu, and B. J. Fraser, Non-Maxwellian particle distributions and electromagnetic ion cyclotron instabilities in the near-Earth magnetotail, *Geophys. Res. Lett., 24*, 2913, 1997.

Chaston, C. C., Y. D. Hu, and B. J. Fraser, Electromagnetic ion cyclotron waves in the near-Earth magnetotail, *J. Geophys. Res., 104*, 6953, 1999a.

Chaston, C. C., Y. D. Hu and B. J. Fraser, Quasi-linear evolution of the ion cyclotron beam anisotropy instability in a current carrying plasma, *Phys. Plasmas, 6*, 2588, 1999b.

Davidson, R. C., D. A. Hamer, I. Haber and C. E. Wagner, Nonlinear development of electromagnetic instabilities in anisotropic plasmas, *Phys. Fluids, 15*, 317, 1972.

Delcourt, D. C., J. A. Savaud, and T. E. Moore, Polar wind dynamics in the magnetotail, *J. Geophys. Res., 98*, 9155, 1993.

Delcourt, D. C., T. E. Moore, and C. R. Chappell, Contribution of low-energy ionospheric protons to the plasma sheet, *J. Geophys. Res., 99*, 5681, 1994.

Eastman, T. E., L. A. Frank, W. K. Peterson, and W. Lennartsson, The plasma sheet boundary layer, *J. Geophys. Res., 89*, 1553, 1984.

Erlandson, R. E., and L. J. Zanetti, A statistical study of auroral electromagnetic ion cyclotron waves, *J. Geophys. Res., 103*, 4627, 1998.

Frank, L. A., W. R. Paterson, K. L Ackerson, S. Kokubun, and T. Yamamoto, Plasma velocity distributions in the near-Earth plasma sheet: A first look with the GEOTAIL spacecraft, *J. Geophys. Res., 101*, 10627, 1996.

Galeev, A. A., and R. Z. Sagdeev, Wave particle interactions, in *Basic Plasma Physics*, vol. 1, chap. 4, pp. 519-586, North-Holland, New York, 1983.

Gary, S. P., *Theory of Space Plasma Microinstabilities, Cambridge Atmos. Space Sci.*, Cambridge Univ. Press, New York, 1993.

Gary, S. P., and R. L. Tokar, The second-order theory of electromagnetic hot ion beam instabilities, *J. Geophys. Res., 90*, 65, 1985.

Gary, S. P., and D. Winske, Computer simulations of electromagnetic instabilities in the plasma sheet boundary layer, *J. Geophys. Res., 95*, 8085, 1990.

Gary, S. P., M. F. Thomsen, L. Yin, and D. Winske, Electromagnetic proton cyclotron instability: interactions with magnetospheric protons, *J. Geophys. Res, 100*, 21,961, 1995.

Gary, S. P., L. Yin, and D. Winske, Electromagnetic proton cyclotron instability: Heating of cool magnetospheric helium ions, *Ann. Geophys., 14*, 1, 1996a.

Gary, S. P., V. M. Vasquez, and D. Winske, Electromagnetic proton cyclotron instability: Proton velocity distributions, *J. Geophys. Res., 101*,13,327, 1996b.

Grabbe, C. L., and T. E. Eastman, Generation of broadband electrostatic noise by ion beam instabilities in the magnetotail, *J. Geophys. Res., 89*, 3865, 1984.

Hirahara, M., T. Mukai, T. Terasawa, S. Machida, Y. Saito, T. Yamamoto, and S. Kokubun, Cold dense ions flows with multiple components observed in the distant tail lobe by GEOTAIL, *J. Geophys. Res., 101*, 7769, 1996.

Huang, C. Y., and L. A. Frank, A statistical survey of the central plasma sheet, *J. Geophys. Res., 99*, 83, 1994.

Kennel, C. F., and H. E. Petschek, Limit on stably trapped particle fluxes, *J. Geophys. Res., 71*, 1, 1966.

Kintner, P. M., M. C. Kelley, R. D. Sharp, A. G. Ghielmetti, M. Temerin, C. A. Cattell, and P. Mizera, Simultaneous observations of energetic (keV) upstreaming ions and EHC waves, *J. Geophys. Res., 84*, 7201, 1979.

Krall, N. A., and A. W. Trivelpiece, *Principles of Plasma Physics*, 674 pp., McGraw-Hill, New York, 1973.

Lennartsson, W., and E. G. Shelley, Survey of 0.1-16 keV/e plasma sheet ion composition, *J. Geophys. Res., 91*, 3061, 1986.

Lennartsson, W., R. D. Sharp, and R. D. Zwickl, Substorm effects on the plasma sheet ion composition on March 22, 1979 (CDAW 6), *J. Geophys. Res.,90*, 1243, 1985.

Lund, E. J., *et al.*, FAST observations of preferentially accelerated He^+ in association with auroral electromagnetic ion cyclotron waves, *Geophys. Res. Lett., 25*, 2049, 1998.

Machida, S. K., C. K. Goertz, and T. Hada, The electromagnetic ion cyclotron instability in the Io torus, *J. Geophys. Res., 93*, 7545, 1988.

Mozer, F. S., C. A Cattell, M. K. Hudson, R. L. Lysak, M. Temerin, and R. B. Torbert, Satellite measurements and theories of low altitude auroral particle acceleration, *Space Sci. Rev., 27*, 155, 1980.

Mozer, F. S., R. Ergun, M. Temerin, C. Cattell, J. Dombeck, and J. Wygant, New features of time domain electric-field structures in the auroral acceleration region, *Phys. Rev. Lett., 79*, 1281, 1997.

Omura, Y., M. Ashour-Abdalla, R. Gendrin, and K. Quest, Heating of thermal helium in the equatorial magnetosphere: A simulation study, *J. Geophys. Res., 90*, 8281, 1985.

Peterson, W. K., R. D. Sharp, E. G. Shelley, and R. G. Johnson, Energetic ion composition of the plasma sheet, *J. Geophys. Res., 86*, 761, 1981.

Seki, K., M. Hirahara, T. Terasawa, T. Mukai, and S. Kokubun, Properties of He^+ beams observed by Geotail in the lobe/mantle regions: Comparison with O^+ beams, *J. Geophys. Res., 104*, 6973, 1999.

Sharp, R. D., D. L. Carr, W. Lennartsson, W. K. Peterson, and E. G. Shelley, Ion streams in the magnetotail, *J. Geophys. Res., 86*, 4639, 1981.

Sharp, R. D., W. Lennartsson, W. K. Peterson, and E. G. Shelley, The origin of plasma in the distant plasma sheet, *J. Geophys. Res., 87*, 10,420, 1982.

Sharp, R. D., R. G. Johnson, W. Lennartsson, W. K. Peterson, and E. G. Shelley, Hot plasma composition results from the ISEE-1 spacecraft, in *Energetic Ion Composition in the Earth's Magnetosphere, Adv. Earth Planet. Sci.*, edited by R. G. Johnson, p. 231, Terra Sci., Tokyo, 1983.

Speiser, T. W., and R. F. Martin, Neutral line energetic ion signatures in the geomagnetic tail: Comparisons with AMPTE observations, in *Space Plasmas: Coupling Between Small and Medium Scale Processes, Geophys. Monogr. Ser.*, vol. 86, edited by M. Ashour-Abdalla, T. Chang, and P. Dusenberry, p. 243, AGU, Washington, D. C., 1995.

Tanaka, M., Simulations of heavy ion heating by electromagnetic ion cyclotron waves driven by temperature anisotropies, *J. Geophys. Res., 90*, 6459, 1985.

Temerin, M., and R. L. Lysak, Electromagnetic ion cyclotron mode (ELF) waves generated by auroral electron precipitation, *J. Geophys. Res., 89*, 2849, 1984.

Tsurutani, B., I. G. Richardson, R. M. Thorne, W. Butler, E. J. Smith, S. W. H. Cowley, S. P. Gary, S.-I. Akasofu, and R. D. Zwickl, Observations of the right-hand resonant ion beam instability in the distant plasma sheet boundary layer, *J. Geophys. Res., 90*, 12,159, 1985.

Winske, D., and N. Omidi, Electromagnetic ion/ion cyclotron instability: Theory and simulations, *J. Geophys. Res., 97*, 14,779, 1992.

Yoon, P.H., C. S. Wu, and M. E Mandt, Ion heating by kinetic cross-field streaming instability due to reflected ions at a quasiperpendicular shock, *Phys. Fluids B, 4*, 719, 1992.

C. C. Chaston, Space Sciences Laboratory, University of California, Berkeley, CA 94720. (ccc@ssl.berkeley.edu)

B. J. Fraser and Y. D. Hu, Physics Department, University of Newcastle, NSW2038, Australia.

(Received June 14, 1999; revised October 20, 1999; accepted October 20, 1999.)